

Manifold Optimization for Hybrid Beamforming in Dual-Function Radar-Communication System

Bowen Wang, *Graduate Student Member, IEEE* Ziyang Cheng, *Member, IEEE* Zishu He, *Senior Member, IEEE*

Abstract—We study hybrid beamforming design for millimeter wave dual-function radar communication system, which simultaneously performs downlink communication and target detection. With two typical analog beamformer structures, we consider the hybrid beamforming design to minimize a weighted summation of radar and communication performance. Leveraging Riemannian optimization theory, a manifold based on the alternating direction method of multipliers is developed for the fully-connected structure. While for the partially-connected structure, a low-complexity Riemannian product manifold trust region algorithm is proposed to approach a near-optimal solution. Numerical simulations are provided to demonstrate the effectiveness of the proposed methods.

Index Terms—Dual-function radar-communication, millimeter wave, hybrid beamforming, product manifold, Riemannian optimization.

I. INTRODUCTION

The increasing number of wireless devices leads to more and more serious spectrum congestion. As a consequence, there is a serious spectrum overlap between different devices, such as airborne radars and navigation systems are close to the 3.4GHz band, which partially overlap with the Long Term Evolution (LTE) systems. Another instance is that the communication satellite (CS) systems and Wi-Fi systems operate in the C-band (4-8 GHz), which is also utilized by the military radars. To address the spectrum congestion between radar and communication, the communication radar spectrum sharing (CRSS) technology is a promising way. The existing works on the CRSS mainly focus on the two aspects.

1) Co-Existence between radar and communication systems

Co-existence between radar and communication systems sharing the same bandwidth has been a primary investigation field in recent years [1]–[5]. The early co-existence work focuses on dynamic spectrum access [1], where the radar or communication works when the other system is in a silent period. Then, benefiting from the cognitive radio development, the design of the spectrum compatible waveform with desired spectral nulls has widely been investigated [3]–[5], which provides a way to achieve co-existence for widely separated spectra systems. However, it is not really an implementation of co-existence between radar and communication. Note that the abovementioned works realize co-existence from radar or communication, which results in a performance loss on another side.

Recently, the joint design scheme of radar and communication systems has become a favorable method for the co-existence systems [6]–[11] by jointly reducing the inter-interference with each other [12], [13]. For example, the authors in [6] propose a co-design of radar sampling matrix and communication codebook to co-exist between matrix completion based MIMO radar and MIMO communication. In addition, some co-design approaches centered on communication performance are suggested in recent studies, wherein anti-radar-interference strategies are taken either at the communication receiver [9] or, using some prior information, directly at the communication transmitter [10], [11]. Although these co-design methods can achieve satisfactory CRSS, the cooperation systems operating in two separated platforms need strict requirements, such as the synchronizations of frequency and sampling times. More importantly, these methods will bring extra hardware costs and complexity.

2) Dual-function radar communication systems

To handle the limitations of the co-existence with two platforms, the dual-function radar communication (DFRC) system, where radar and communication share in a common platform, has been regarded as a more promising approach to realize the CRSS [14]–[23]. Pioneering effort [14] considers the single-antenna system, in which several integrated waveforms that can achieve both radar and communication functions are presented. However, these methods will result in a performance loss for radar and communication because of lacking of degree of freedoms (DOFs). As a step further, more recent works focus on the DFRC based on the MIMO systems. For example, a DFRC system utilizing waveform diversity in tandem with amplitude/phase control has been introduced in a number of papers [15], [16]. Moreover, the authors in [18], [19] investigate radar-embedded communications on an intrapulse, which allows for low-probability-of-intercept communication and enjoys high target detection performance [19]. To exploit the available frequency spectrum more efficiently, the authors in [22] investigate the DFRC waveform design in full-Duplex mode. Additionally, a common waveform is devised to communicate with the downlink multi-user and detect radar targets in [17], in which the trade-off problem between radar and communication is established by minimize the downlink multi-user interference (MUI) under radar-specific constraints.

It should be noted that the above methods adopt the conventional fully-digital beamforming schemes, where each antenna requires a radio frequency (RF) chain (including a Digital-to-Analog converter, up converter, etc.), leading to high hardware cost and power consumption, particularly in large-scale array systems, such as millimeter wave (mmWave) systems.

B. Wang, Z. Cheng and Z. He are with School of Information and Communication Engineering, University of Electronic Science and Technology of China, Chengdu 611731, China (B_W_Wang@163.com, {zycheng, zshe}@uestc.edu.cn). (Corresponding author: Ziyang Cheng.)

Towards system energy efficiency, hybrid beamforming (HBF) architecture consisting of analog and digital beamformers is widely studied for mmWave massive MIMO systems [24]–[29], in which a small number of RF chains is utilized to implement the digital beamformer and a large number of phase shifters (PSs) to realize the analog beamformer. According to the mapping from the RF chain to antennas, the hybrid beamforming architectures can be categorized into fully-connected and partially-connected (sub-connected) structures, as shown in Fig.1(a) and Fig.1(b), respectively. Compared with the fully-connected structure, the partially-connected structure, where each RF chain is connected to only a subset of antennas, is more low-cost and power efficient with slight performance loss.

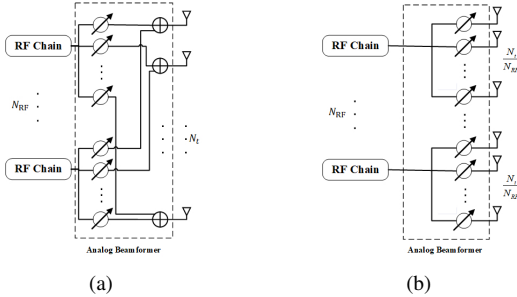


Fig. 1. Two structures of hybrid beamforming in mmWave MIMO systems. (a) Fully-connected structure; (b) Partially-connected structure.

It is worth pointing out that all the works above on the hybrid beamforming design focus on the communication systems. Recently, many researchers have devoted themselves to the hybrid beamforming design for the mmWave DFRC system [30]–[34]. The mmWave DFRC system adopting a hybrid beamforming structure is first presented in [30], where a weighting problem is derived to facilitate the trade-off between MIMO radar and mmWave communication. Moreover, the authors in [31] propose to jointly design the analog and digital beamformer for mmWave wideband Orthogonal Frequency Division Multiplexing (OFDM) DFRC system. However, these works focus on designing the analog beamformer by exploiting the block coordinate descent (BCD) method, which may lead to performance loss. More importantly, the BCD method has a high computational complexity, which is unsuitable for the large-scale array.

More recently, manifold optimization has been vigorously developed and widely used in radar and communication designs [35]–[40]. It converts the non-convex constraint, like constant modulus, Grassmann and Stiefel, into the corresponding manifold and performs the optimization on the manifold space [36]. Moreover, many optimization solvers are based on manifold gradients, which enjoy high convergence speed and low complexity [35]–[37].

This motivates us to study the design of analog and digital beamformers in DFRC systems via manifold minimization. The contributions of this paper can be summarized as follows.

- The problems of the hybrid beamforming design of the DFRC system with the fully-connected and partially-connected structures are formulated by considering an

optimization criterion of a weighted summation of the communication and radar beamforming errors.

- For the fully-connected structure, we propose the manifold alternating direction method of multipliers (MADMM) framework to tackle the hybrid beamforming optimization problem. To be more specific, we decouple the digital and analog beamformers by using the ADMM framework, such that we can optimize the digital and analog beamformers independently. Moreover, the sub-problem of updating analog beamformer is suboptimally solved by utilizing the Manifold optimization with a low-complexity.
- For the partially-connected structure, we propose the Riemannian product manifold (RPM) optimization framework for the joint design of analog and digital beamforming. Based on the manifold optimization, the constrained optimization problem reformulate as a unconstrained optimization problem, via transforming the constant modulus and transmit power constraints into feasible search region. We derive the expressions of the Riemannian product gradient and Hessian informations, and present the trust region (TR) algorithm to obtain the near-optimal solution.

The rest of the paper is organized as follows. In Section II, we introduce the system model for the mmWave DFRC system with hybrid beamforming structure. In Section III, we formulate our problem by considering the trade-off designs between radar and communication. In Section IV, an efficient MADMM algorithm for the hybrid beamforming with fully-connected structure is presented. In Section V, we propose the Riemannian product manifold trust region algorithm (RPM-TR) to design the hybrid beamformer with partially-connected structure. In Section VI, we analyze the numerical performance of the proposed algorithms and compare our approaches with the existing methods. Finally, we draw several conclusions in Section VII.

Notions: Unless otherwise specified, matrices are denoted by bold uppercase letters (i.e., \mathbf{H}), bold lowercase letters are used for vectors (i.e., $\boldsymbol{\alpha}$), scalars are denoted by normal font (i.e., β). $(\cdot)^T$, $(\cdot)^*$ and $(\cdot)^H$ represent the transpose, complex conjugate and Hermitian transpose respectively. The set of n -dimensional complex-valued (real-valued) vector and $N \times N$ complex-valued (real valued) matrices are denoted by \mathbb{C}^n (\mathbb{R}^n) and $\mathbb{C}^{N \times N}$ ($\mathbb{R}^{N \times N}$), respectively. \otimes and \circ denote the Kronecker and Hadamard products between two matrices. $|\cdot|$ and $\|\cdot\|_F$ represent determinant and Frobenius norm of argument, respectively. $\text{vec}(\cdot)$ and $\text{tr}(\cdot)$ stand for the vectorization and trace of the argument, respectively. $\Re(\cdot)$ denotes the real part of argument, and \mathbb{E} represents expectation of a complex variable.

II. SYSTEM MODEL

Consider a mmWave MIMO-DFRC system, which transmits probing signals to targets of interest and sends communication symbols to downlink user simultaneously. As shown in Fig.2, the joint transmit system is equipped with N_{RF} RF chains and N_t antennas, which attempts to send N_s data streams to a

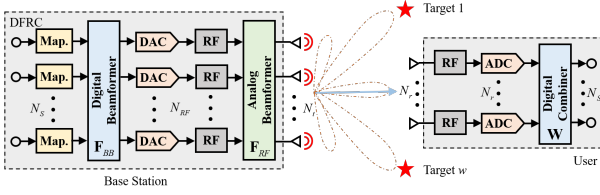


Fig. 2. Overview of a mmWave dual-functional radar-communication system with hybrid analog and digital beamforming architecture at the transmitter (base station).

downlink user with N_r antennas. Both the DFRC transmit and downlink user receive arrays are assumed to be half-wavelength spaced uniform linear arrays (ULA). In our consideration, we assume that the number of RF chains is smaller than that of antennas at the transmit end.

A. Communication Model

In hybrid beamforming system, the data stream \mathbf{s} is first processed by a digital beamformer $\mathbf{F}_{BB} \in \mathbb{C}^{N_{RF} \times N_s}$, and then up-converted to the carrier frequency by passing through N_{RF} radio frequency (RF) chains. After that, the DFRC system uses an $\mathbf{F}_{RF} \in \mathbb{C}^{N_t \times N_{RF}}$ RF beamformer, which is implemented using analog phase shifters, to construct the final transmitted signal. Mathematically, the $N_t \times 1$ transmitted signal can be written as

$$\mathbf{x} = \mathbf{F}_{RF} \mathbf{F}_{BB} \mathbf{s} \quad (1)$$

where, $\mathbf{s} \in \mathbb{C}^{N_s \times 1}$ is the transmitted symbol vector in the baseband. Furthermore, it is assumed that $\mathbb{E}(\mathbf{s} \mathbf{s}^H) = \frac{1}{N_s} \mathbf{I}_{N_s}$ [29]. The transmitter should satisfy the transmission power constraint, i.e., $\|\mathbf{F}_{RF} \mathbf{F}_{BB}\|_F^2 = N_s$.

The received signal at the downlink user can be expressed as

$$\mathbf{y} = \sqrt{\rho} \mathbf{H} \mathbf{F}_{RF} \mathbf{F}_{BB} \mathbf{s} + \mathbf{n} \quad (2)$$

where ρ denotes the average received power, $\mathbf{H} \in \mathbb{C}^{N_r \times N_t}$ is the downlink channel matrix, and \mathbf{n} denotes the white Gaussian noise with zero mean and variance σ_n^2 .

Furthermore, there are several mapping strategies from RF chains to antennas, here we consider the fully-connected and partially-connected structures, as illustrated in Fig.1(a) and Fig.1(b). For the fully-connected structure, the RF chains are connected to all antennas, i.e. $|\mathbf{F}_{RF}(i, j)| = 1, \forall i, j$. While for the partially-connected structure, we assume each RF chain is connected to N_t/N_{RF} antennas, such that we have $\mathbf{F}_{RF} = \text{diag}[\mathbf{f}_{RF1}, \mathbf{f}_{RF2}, \dots, \mathbf{f}_{RFN_{RF}}]$, where \mathbf{f}_{RFn} is an N_t/N_{RF} dimensional vector whose each element has a constant modulus.

To incorporate the high free-space path loss and limited scattering characteristics of the mmWave channels, we adopt a clustered channel model, i.e. Saleh-Valenzuela model [24]–[29]. Under this model, the channel matrix can be written as

$$\mathbf{H} = \sqrt{\frac{N_t N_r}{N_{cl} N_{ray}}} \sum_{i=1}^{N_{cl}} \sum_{l=1}^{N_{ray}} \alpha_{il} \mathbf{a}_r(\phi_{il}^r) \mathbf{a}_t(\phi_{il}^t)^H \quad (3)$$

where N_{cl} and N_{ray} represent the number of clusters and the number of rays in each cluster, and α_{il} denotes the gain of l th ray in the i th propagation cluster. In addition, $\mathbf{a}_r(\phi_{il}^r)$ and $\mathbf{a}_t(\phi_{il}^t)$ represent the receive and transmit array response vectors, where ϕ_{il}^r and ϕ_{il}^t stand for azimuth angles of arrival and departure (AoAs and AoDs), respectively. Under the ULA assumption with half waveform length element spacing, the receive and transmit array response vectors can be expressed as

$$\begin{aligned} \mathbf{a}_r(\phi) &= \frac{1}{\sqrt{N_r}} \left[1, e^{j\pi \sin \phi}, \dots, e^{j\pi(N_r-1) \sin \phi} \right]^T, \\ \mathbf{a}_t(\phi) &= \frac{1}{\sqrt{N_t}} \left[1, e^{j\pi \sin \phi}, \dots, e^{j\pi(N_t-1) \sin \phi} \right]^T. \end{aligned} \quad (4)$$

In this paper, we assume that perfect channel state information (CSI) is known at the transmitter. Then, the channel's mutual information can be presented as [24]–[29]

$$R = \log_2 \left(\mathbf{I}_{N_r} + \frac{\rho}{N_s \sigma_n^2} \mathbf{H} \mathbf{F}_{RF} \mathbf{F}_{BB} \mathbf{F}_{BB}^H \mathbf{F}_{RF}^H \mathbf{H}^H \right) \quad (5)$$

B. Radar Model

In addition to downlink communication, the DFRC system aims to detect the targets of interest. In particular, we consider a typical radar scenario, where many targets of interest exist without the signal-dependent clutter. The baseband signal radiated towards a target located at the direction θ can be described as

$$z(\theta) = \mathbf{a}_t^H(\theta) \mathbf{F} \mathbf{s} \quad (6)$$

where $\mathbf{F} = \mathbf{F}_{RF} \mathbf{F}_{BB}$ and $\mathbf{a}_t(\theta)$ has the similar form as (4).

According to (6), the transmit beampattern of radar can be given as

$$P(\theta) = \frac{1}{N_s} \mathbf{a}_t^H(\theta) \mathbf{F} \mathbf{F}^H \mathbf{a}_t(\theta) = \frac{1}{N_s} \mathbf{f}^H \mathbf{Q}(\theta) \mathbf{f} \quad (7)$$

where $\mathbf{f} \triangleq \text{vec}(\mathbf{F}) = \text{vec}(\mathbf{F}_{RF} \mathbf{F}_{BB})$ and the matrix $\mathbf{Q}(\theta)$ is given by

$$\mathbf{Q}(\theta) = \mathbf{I}_{N_s} \otimes \left(\mathbf{a}_t(\theta) \mathbf{a}_t^H(\theta) \right) \in \mathbb{C}^{N_t N_s \times N_t N_s} \quad (8)$$

In order to improve the detection performance, it is desired to focus on the transmit power at the locations of the targets of interest and to minimize the power at the sidelobes. For this purpose, we use integrated sidelobe to mainlobe ratio (ISMR) [41], [42] as an indicator to measure the property of the transmit beampattern, that is

$$\text{ISMR} = \frac{\int_{\Theta_s} P(\theta) d\theta}{\int_{\Theta_m} P(\theta) d\theta} = \frac{\mathbf{f}^H \mathbf{L}_s \mathbf{f}}{\mathbf{f}^H \mathbf{L}_m \mathbf{f}} \quad (9)$$

where Θ_s and Θ_m represent the sidelobe and mainlobe regions, respectively. \mathbf{L}_s and \mathbf{L}_m are defined as

$$\mathbf{L}_s = \int_{\Theta_s} \mathbf{Q}(\theta) d\theta \quad \text{and} \quad \mathbf{L}_m = \int_{\Theta_m} \mathbf{Q}(\theta) d\theta \quad (10)$$

III. PROBLEM FORMULATION

In this section, we first present the hybrid beamforming design for communication-only case and radar-only case, respectively. Then, based on the two special cases, we formulate

a weighted summation problem to achieve a good trade-off between radar and communication for the DFRC system.

A. Hybrid Beamforming for Communication-Only System

In general, communication system need to maximize the mutual information to guarantee the quality of service (QoS). In this paper, we mainly focus on the beamformer design and assume the receiver equipping with an ideal (fully-digital) decoders. Following this strategy, the problem of the hybrid beamformer design for the communication-only system can be established as

$$\begin{aligned} \max_{\mathbf{F}_{RF}, \mathbf{F}_{BB}} R &= \log_2 \left(\mathbf{I}_{N_r} + \frac{\rho}{N_s \sigma_n^2} \mathbf{H} \mathbf{F}_{RF} \mathbf{F}_{BB} \mathbf{F}_{BB}^H \mathbf{F}_{RF}^H \mathbf{H}^H \right) \\ \text{s.t.} \quad & \|\mathbf{F}_{RF} \mathbf{F}_{BB}\|_F^2 = N_s \\ & |\mathbf{F}_{RF}(i, j)| = 1, \forall (i, j) \in \mathcal{A} \end{aligned} \quad (11)$$

where \mathcal{A} is the feasible set of the analog precoder. Due to the nonconvexity of the objective function in (11), the problem is difficult to solve numerically. Nevertheless, it has been shown in [29] that maximizing the objective function in (11) approximately leads to the minimization of the following problem:

$$\begin{aligned} \min_{\mathbf{F}_{RF}, \mathbf{F}_{BB}} & \|\mathbf{F}_{RF} \mathbf{F}_{BB} - \mathbf{F}_{Com}\|_F^2 \\ \text{s.t.} \quad & \|\mathbf{F}_{RF} \mathbf{F}_{BB}\|_F^2 = N_s \\ & |\mathbf{F}_{RF}(i, j)| = 1, \forall (i, j) \in \mathcal{A} \end{aligned} \quad (12)$$

where \mathbf{F}_{Com} denotes the optimal fully digital precoder, which can be obtained by various approaches [29]. Here, this paper adopts zero-forcing (ZF) method to calculated it, as

$$\mathbf{F}_{Com} = \frac{1}{\sqrt{\text{tr}(\mathbf{H}\mathbf{H}^H)^{-1}}} \mathbf{H}^H (\mathbf{H}\mathbf{H}^H)^{-1} \quad (13)$$

B. Hybrid Beamforming for Radar-Only System

On the other hand, for the radar-only system, the transmit beamformer is desired to carefully design to attain the minimum ISMR, the corresponding optimization problem is formulated as

$$\min_{\mathbf{f}} \text{ISMR} = \frac{\mathbf{f}^H \mathbf{L}_s \mathbf{f}}{\mathbf{f}^H \mathbf{L}_m \mathbf{f}} \quad \text{s.t.} \quad \|\mathbf{f}\|_F^2 = N_s \quad (14)$$

whose optimal solution can be achieved by taking the generalized eigenvalue decomposition of $(\mathbf{L}_m, \mathbf{L}_s)$ [41], i.e.

$$\mathbf{f}_{Rad} = \mathcal{P}(\mathbf{L}_s^{-1} \mathbf{L}_m) \quad (15)$$

where the operator $\mathcal{P}(\cdot)$ denotes the principal eigenvector. In order to satisfy the power constraint in (14), the \mathbf{f}_{Rad} should be scaled as $\sqrt{N_s} \frac{\mathbf{f}_{Rad}}{\|\mathbf{f}_{Rad}\|} \rightarrow \mathbf{f}_{Rad}$.

Similarly to the communication-only case, the hybrid beamformer is designed by considering the following surrogate function:

$$\begin{aligned} \min_{\mathbf{F}_{RF}, \mathbf{F}_{BB}} & \|\mathbf{F}_{RF} \mathbf{F}_{BB} - \mathbf{F}_{Rad}\|_F^2 \\ \text{s.t.} \quad & \|\mathbf{F}_{RF} \mathbf{F}_{BB}\|_F^2 = N_s \\ & |\mathbf{F}_{RF}(i, j)| = 1, \forall (i, j) \in \mathcal{A} \end{aligned} \quad (16)$$

where \mathbf{F}_{Rad} is the matrix form of \mathbf{f}_{Rad} .

C. Hybrid Beamforming for DRFC System

In DFRC system, our aim is to design the hybrid beamformer to ensure not only the high-quality for communication, but also the detection performance for radar. To achieve thus purpose, we introduce a weighted summation of the communication and radar beamforming errors as the optimization objective, and the resultant problem can be formulated as

$$\begin{aligned} \min_{\mathbf{F}_{RF}, \mathbf{F}_{BB}} & \varphi \|\mathbf{F}_{RF} \mathbf{F}_{BB} - \mathbf{F}_{Com}\|_F^2 \\ & + (1 - \varphi) \|\mathbf{F}_{RF} \mathbf{F}_{BB} - \mathbf{F}_{Rad}\|_F^2 \end{aligned} \quad (17a)$$

$$\text{s.t.} \quad \|\mathbf{F}_{RF} \mathbf{F}_{BB}\|_F^2 = N_s \quad (17b)$$

$$|\mathbf{F}_{RF}(i, j)| = 1, \forall (i, j) \in \mathcal{A} \quad (17c)$$

where $\varphi \in [0, 1]$ is a weighting factor (trade-off parameter) that determines the weights for communication and radar performance. In Sections IV and V, we will consider the RF beamformer designs for the fully-connected structure and partially-connected structure, respectively. It is noticed that the problem (17) is difficult to tackle due to the nonconvex constraints. Nevertheless, we note that the feasible region in problem (17) satisfies the manifold constraints. Consequently, in the following, we propose to solve the nonconvex problem (17) with the aid of the Riemannian optimization algorithms [35]–[37], which finds a suboptimal solution with low-complexity.

IV. MADMM BASED HYBRID BEAMFORMING FOR THE FULLY-CONNECTED STRUCTURE

In this section, we consider the hybrid beamforming design for the fully-connected structure. In order to obtain a near-optimal solution to the problem (17) with the constraint $|\mathbf{F}_{RF}(i, j)| = 1, \forall i, j$, the manifold alternating direction method of multipliers (MADMM) is proposed.

A. MADMM algorithm

As discussed in [43] that solving problem (17) with the ADMM framework needs to decouple \mathbf{F}_{RF} and \mathbf{F}_{BB} in constraint (17b). To attain such purpose, we introduce an auxiliary variable \mathbf{F} , and recast the problem (17) as the following problem:

$$\begin{aligned} \min_{\mathbf{F}_{RF}, \mathbf{F}_{BB}} & \varphi \|\mathbf{F} - \mathbf{F}_{Com}\|_F^2 + (1 - \varphi) \|\mathbf{F} - \mathbf{F}_{Rad}\|_F^2 \\ \text{s.t.} \quad & \mathbf{F} = \mathbf{F}_{RF} \mathbf{F}_{BB} \\ & \|\mathbf{F}\|_F^2 = N_s \\ & |\mathbf{F}_{RF}(i, j)| = 1, \forall i, j \end{aligned} \quad (18)$$

This will enable us to solve the problem (18) more easily under the ADMM framework. Specifically, placing the equality constraint $\mathbf{F} = \mathbf{F}_{RF} \mathbf{F}_{BB}$ into the augmented Lagrangian function yields

$$\begin{aligned} \mathcal{L}(\mathbf{F}, \mathbf{F}_{RF}, \mathbf{F}_{BB}, \boldsymbol{\Lambda}) &= \varphi \|\mathbf{F} - \mathbf{F}_{Com}\|_F^2 + (1 - \varphi) \|\mathbf{F} - \mathbf{F}_{Rad}\|_F^2 \\ & + \frac{\alpha}{2} \left\| \mathbf{F} + \frac{\boldsymbol{\Lambda}}{\alpha} - \mathbf{F}_{RF} \mathbf{F}_{BB} \right\|_F^2 \end{aligned} \quad (19)$$

Under the ADMM framework, the solution of (18) can be obtained via minimizing the Lagrangian function (19). Now the constraints for each variable are separated, and the coordinate descent (CD) algorithm can be utilized to solve for the variables \mathbf{F} , \mathbf{F}_{RF} and \mathbf{F}_{BB} iteratively. In the following subsection, we will discuss the solution for each block in detail.

• **Update of \mathbf{F}**

For the fixed $\{\mathbf{F}_{RF}^{(n-1)}, \mathbf{F}_{BB}^{(n-1)}, \mathbf{\Lambda}^{(n-1)}\}$, the problem of updating the \mathbf{F} is given by

$$\begin{aligned} \min_{\mathbf{F}} \quad & \varphi \|\mathbf{F} - \mathbf{F}_{Com}\|_F^2 + (1 - \varphi) \|\mathbf{F} - \mathbf{F}_{Rad}\|_F^2 \\ & + \frac{\alpha}{2} \left\| \mathbf{F} + \frac{\mathbf{\Lambda}^{(n-1)}}{\alpha} - \mathbf{F}_{RF}^{(n-1)} \mathbf{F}_{BB}^{(n-1)} \right\|_F^2 \\ \text{s.t.} \quad & \|\mathbf{F}\|_F^2 = N_S \end{aligned} \quad (20)$$

We note that its closed form solution can be attained by using the Karush-Kuhn-Tucker (KKT) conditions. Specifically, introducing a Lagrange multiplier Φ on the power constraint, we obtain the following Lagrange function:

$$\begin{aligned} \mathcal{K}(\mathbf{F}, \Phi) = & \varphi \|\mathbf{F} - \mathbf{F}_{Com}\|_F^2 + (1 - \varphi) \|\mathbf{F} - \mathbf{F}_{Rad}\|_F^2 \\ & + \frac{\alpha}{2} \left\| \mathbf{F} + \frac{\mathbf{\Lambda}^{(n-1)}}{\alpha} - \mathbf{F}_{RF}^{(n-1)} \mathbf{F}_{BB}^{(n-1)} \right\|_F^2 + \Phi \left(\|\mathbf{F}\|_F^2 - N_S \right) \end{aligned} \quad (21)$$

Based on the Lagrangian in (21), the KKT conditions for optimality are then obtained as

$$\frac{\partial \mathcal{K}}{\partial \mathbf{F}} = 2\varphi(\mathbf{F} - \mathbf{F}_{Com}) + 2(1 - \varphi)(\mathbf{F} - \mathbf{F}_{Rad}) + \alpha \left(\mathbf{F} + \frac{\mathbf{\Lambda}^{(n-1)}}{\alpha} - \mathbf{F}_{RF}^{(n-1)} \mathbf{F}_{BB}^{(n-1)} \right) + 2\Phi \mathbf{F} = 0 \quad (22a)$$

$$\Phi \left(\|\mathbf{F}\|_F^2 - N_S \right) = 0 \quad (22b)$$

$$\Phi \geq 0 \quad (22c)$$

Hence, based on the KKT conditions, the closed-form solution to \mathbf{F} is given by

$$\mathbf{F}_{opt} = \sqrt{N_S} \frac{\bar{\mathbf{F}}}{\|\bar{\mathbf{F}}\|_F} \quad (23)$$

where $\bar{\mathbf{F}} = 2\varphi \mathbf{F}_{Com} + 2(1 - \varphi) \mathbf{F}_{Rad} - \alpha \left(\frac{\mathbf{\Lambda}^{(n-1)}}{\alpha} - \mathbf{F}_{RF}^{(n-1)} \mathbf{F}_{BB}^{(n-1)} \right)$.

• **Update of \mathbf{F}_{RF}**

For fixed $\{\mathbf{F}^{(n)}, \mathbf{F}_{BB}^{(n-1)}, \mathbf{\Lambda}^{(n-1)}\}$, the problem of updating the \mathbf{F}_{RF} can be formulated as

$$\begin{aligned} \min_{\mathbf{F}_{RF}} \quad & \left\| \mathbf{F}^{(n)} + \frac{\mathbf{\Lambda}^{(n-1)}}{\alpha} - \mathbf{F}_{RF} \mathbf{F}_{BB}^{(n-1)} \right\|_F^2 \\ \text{s.t.} \quad & |\mathbf{F}_{RF}(i, j)| = 1, \forall i, j \end{aligned} \quad (24)$$

Based on the manifold optimization in [35]–[37], problem (24) can be converted into the unconstrained optimization problem over manifold, given by

$$\min_{\mathbf{F}_{RF} \in \mathcal{M}_{\mathbf{F}_{RF}}} g(\mathbf{F}_{RF}) = \left\| \mathbf{F}^{(n)} + \frac{\mathbf{\Lambda}^{(n-1)}}{\alpha} - \mathbf{F}_{RF} \mathbf{F}_{BB}^{(n-1)} \right\|_F^2 \quad (25)$$

where $\mathcal{M}_{\mathbf{F}_{RF}}$ denotes an $N_t \times N_{RF}$ dimensional *complex circle manifold* with the geometric structure being given by

$$\mathcal{M}_{\mathbf{F}_{RF}} = \{\mathbf{F}_{RF} \in \mathbb{C}^{N_t \times N_{RF}} : |\mathbf{F}_{RF}(i, j)| = 1, \forall i, j\} \quad (26)$$

Following [35], [36], in order to utilize the Riemannian optimization methods, we need to define a tangent space which is a linear space around any point on a smooth manifold. More concretely, the tangent space $T_{\mathbf{F}_{RF}} \mathcal{M}_{\mathbf{F}_{RF}}$ at the point $\mathbf{F}_{RF} \in \mathcal{M}_{\mathbf{F}_{RF}}$ is defined as

$$T_{\mathbf{F}_{RF}} \mathcal{M}_{\mathbf{F}_{RF}} = \{\mathbf{v} \in \mathbb{C}^{N_{RF} \times N_t} : \Re(\mathbf{v} \circ \mathbf{F}_{RF}^*) = \mathbf{0}\} \quad (27)$$

where \mathbf{v} denotes the tangent vector at point $\mathbf{F}_{RF} \in \mathcal{M}_{\mathbf{F}_{RF}}$.

According to the [35], the Riemannian gradient of $\mathcal{M}_{\mathbf{F}_{RF}}$ at \mathbf{F}_{RF} is a tangent vector $\text{grad}g(\mathbf{F}_{RF})$ given by the projection of the Euclidean gradient $\text{Grad}g(\mathbf{F}_{RF})$ on the the tangent space $T_{\mathbf{F}_{RF}} \mathcal{M}_{\mathbf{F}_{RF}}$:

$$\begin{aligned} \text{grad}g(\mathbf{F}_{RF}) = & \text{Proj}_{T_{\mathbf{F}_{RF}}}(\text{Grad}g(\mathbf{F}_{RF})) \\ = & \text{Grad}g(\mathbf{F}_{RF}) - \Re(\text{Grad}g(\mathbf{F}_{RF})^* \circ \mathbf{F}_{RF}) \circ \mathbf{F}_{RF} \end{aligned} \quad (28)$$

where the Euclidean gradient $\text{Grad}g(\mathbf{F}_{RF})$ is expressed as

$$\text{Grad}g(\mathbf{F}_{RF}) = -2 \left(\mathbf{F}^{(n)} + \frac{\mathbf{\Lambda}^{(n-1)}}{\alpha} - \mathbf{F}_{RF} \mathbf{F}_{BB}^{(n-1)} \right) \left(\mathbf{F}_{BB}^{(n-1)} \right)^H \quad (29)$$

Based on the above Riemannian gradients, in what follow, we propose an Riemannian Conjugate Gradient (RCG) algorithm, which obtains the near-optimal solution with much lower complexity [35], to solve the problem (24). For RCG method, the beamforming matrix to be updated at each iteration is computed by the descent direction and stepsize. In the k -th iteration, the search direction $\mathbf{\Gamma}_{\mathbf{F}_{RF}}^{(k)}$ is determined by the Riemannian gradient $\text{grad}g(\mathbf{F}_{RF}^{(k)})$ and the $(k-1)$ -th search direction $\mathbf{\Gamma}_{\mathbf{F}_{RF}}^{(k-1)}$, which is given by

$$\mathbf{\Gamma}_{\mathbf{F}_{RF}}^{(k)} = -\text{grad}g(\mathbf{F}_{RF}^{(k)}) + \sigma_{\mathbf{F}_{RF}}^{(k-1)} \text{Proj}_{T_{\mathbf{F}_{RF}}^{(k)}}(\mathbf{\Gamma}_{\mathbf{F}_{RF}}^{(k-1)}) \quad (30)$$

where $\sigma_{\mathbf{F}_{RF}}$ is the polak-Ribiere parameter [39], defined as

$$\sigma_{\mathbf{F}_{RF}}^{(k)} = \frac{\langle \text{grad}g(\mathbf{F}_{RF}^{(k)}), \mathbf{\chi}_{\mathbf{F}_{RF}}^{(k)} \rangle}{\langle \text{grad}g(\mathbf{F}_{RF}^{(k-1)}), \text{grad}g(\mathbf{F}_{RF}^{(k-1)}) \rangle} \quad (31)$$

with $\langle \cdot, \cdot \rangle$ denoting the usual Euclidean inner product, i.e., $\langle \mathbf{P}, \mathbf{Q} \rangle = \Re(\text{tr}(\mathbf{P}^H \mathbf{Q}))$, and $\mathbf{\chi}_{\mathbf{F}_{RF}}$ standing for the difference between the current and the previous gradients, and it is expressed as

$$\mathbf{\chi}_{\mathbf{F}_{RF}}^{(k)} = \text{grad}g(\mathbf{F}_{RF}^{(k)}) - \text{Proj}_{T_{\mathbf{F}_{RF}}^{(k-1)}}(\text{grad}g(\mathbf{F}_{RF}^{(k-1)})) \quad (32)$$

Then, the stepsize $\mu_{\mathbf{F}_{RF}}^{(k)}$ is chosen by the Armijo backtrack-ing line search method [39], and the beamforming matrix $\mathbf{F}_{RF}^{(k)}$ to be updated at the step $(k+1)$ is calculated by the *retraction* on the manifold, which is

$$\mathbf{F}_{RF}^{(k+1)} = \mathcal{R}_{\mathbf{F}_{RF}^{(k)}}(\mu_{\mathbf{F}_{RF}}^{(k)} \mathbf{\Gamma}_{\mathbf{F}_{RF}}^{(k)}) \quad (33)$$

where \mathcal{R} is a mapping operator, named as retraction, which maps a vector from the tangent space onto the manifold itself,

given by

$$\begin{aligned} & \mathcal{R}_{\mathbf{F}_{RF}}(\mu_{\mathbf{F}_{RF}} \mathbf{\Gamma}_{\mathbf{F}_{RF}}) \\ &= (\mathbf{F}_{RF} + \mu_{\mathbf{F}_{RF}} \mathbf{\Gamma}_{\mathbf{F}_{RF}}) \circ \frac{1}{|(\mathbf{F}_{RF} + \mu_{\mathbf{F}_{RF}} \mathbf{\Gamma}_{\mathbf{F}_{RF}})|} \end{aligned} \quad (34)$$

Based on the above analysis, the RCG Algorithm for solving (24) is summarized by Algorithm 1.

Algorithm 1 RCG Algorithm for solving (24)

Require: Set the initial variables $\mathbf{F}^{(n)}$, $\mathbf{F}_{BB}^{(n-1)}$, $\mathbf{\Lambda}^{(n-1)}$, \mathbf{F}_{Rad} , \mathbf{F}_{Com} , α and η and K_{max} .

Ensure: $\mathbf{F}_{RF}^{(opt)}$.

- 1: **Initialization:** Randomly set $\mathbf{F}_{RF}^{(0)} \in \mathcal{M}_{\mathbf{F}_{RF}}$
 - 2: Set $k = 1$.
 - 3: **while** $k \leq K_{max}$ and $\|\text{grad}_g(\mathbf{F}_{RF}^{(k)})\|_F \geq \eta$ **do**
 - 4: Compute the stepsize $\mu_{\mathbf{F}_{RF}}^{(k)}$ using the Armijo Rule.
 - 5: Calculate the Polak-Ribiere parameter based on (31).
 - 6: Obtain the descent direction according to (30).
 - 7: Update the beamforming matrix $\mathbf{F}_{RF}^{(k+1)}$ by (33).
 - 8: $k = k + 1$
 - 9: **end while**
 - 10: $\mathbf{F}_{RF}^{(opt)} = \mathbf{F}_{RF}^{(k)}$
-

• **Update of \mathbf{F}_{BB}**

For fixed $\{\mathbf{F}^{(n)}, \mathbf{F}_{RF}^{(n)}, \mathbf{\Lambda}^{(n-1)}\}$, the problem of updating the \mathbf{F}_{BB} can be expressed as

$$\min_{\mathbf{F}_{BB}} \left\| \mathbf{F}^{(n)} + \frac{\mathbf{\Lambda}^{(n-1)}}{\alpha} - \mathbf{F}_{RF}^{(n)} \mathbf{F}_{BB} \right\|_F^2 \quad (35)$$

It is easy to observe that the problem (35) is convex Quadratic Program without constraint, and its closed-form solution can be attained as

$$\mathbf{F}_{BB}^{(n)} = \left((\mathbf{F}_{RF}^{(n)})^H \mathbf{F}_{RF}^{(n)} \right)^{-1} (\mathbf{F}_{RF}^{(n)})^H \left(\mathbf{F}^{(n)} + \frac{\mathbf{\Lambda}^{(n-1)}}{\alpha} \right) \quad (36)$$

• **Update Penalty Parameter α**

In conventional ADMM algorithm [43], using a fixed penalty parameter may lead to poor convergence performance. In order to improve the convergence and make performance less dependent on the initial choice of the penalty parameter, we use the following update scheme of α [43]:

$$\alpha^{(n)} = \begin{cases} \beta \alpha^{(n-1)}, & \text{if } \frac{\|\mathbf{F}^{(n)} - \mathbf{F}_{RF}^{(n)} \mathbf{F}_{BB}^{(n)}\|_F^2}{\|\mathbf{\Lambda}^{(n)} - \mathbf{\Lambda}^{(n-1)}\|_F^2} > \gamma \\ \alpha^{(n-1)} / \beta, & \text{if } \frac{\|\mathbf{F}^{(n)} - \mathbf{F}_{RF}^{(n)} \mathbf{F}_{BB}^{(n)}\|_F^2}{\|\mathbf{\Lambda}^{(n)} - \mathbf{\Lambda}^{(n-1)}\|_F^2} < \frac{1}{\gamma} \\ \alpha^{(n-1)}, & \text{otherwise} \end{cases} \quad (37)$$

where $\beta > 1$ and $\gamma > 1$. In our case, we set $\beta = 2$ and $\gamma = 10$.

According to the above analysis, the proposed method for designing the hybrid beamforming in the case of fully-connected structure is summarized in Algorithm 2.

At the end of this section, we analyze the complexity of the proposed MADMM algorithm for the hybrid beamforming in the case of fully-connected structure. It should be noted that

Algorithm 2 MADMM for fully-connected structure hybrid beamforming design

Require: Set the initial variables \mathbf{F}^0 , \mathbf{F}_{RF}^0 , \mathbf{F}_{BB}^0 , $\mathbf{\Lambda}^0$, α^0 , \mathbf{F}_{Rad} , \mathbf{F}_{Com} and N_{max} .

Ensure: $\mathbf{F}_{RF}^{(opt)}$ and $\mathbf{F}_{BB}^{(opt)}$.

- 1: **Initialization:** Set $n = 1$, $\beta = 2$ and $\gamma = 10$.
 - 2: **while** $n \leq N_{max}$ **do**
 - 3: For given $\mathbf{F}_{RF}^{(n-1)}$, $\mathbf{F}_{BB}^{(n-1)}$, $\mathbf{\Lambda}^{(n-1)}$, obtain the solution of $\mathbf{F}^{(n)}$ by using (23)
 - 4: For given $\mathbf{F}^{(n)}$, $\mathbf{F}_{BB}^{(n-1)}$, $\mathbf{\Lambda}^{(n-1)}$, obtain the solution of $\mathbf{F}_{RF}^{(n)}$ according to Algorithm 1.
 - 5: For given $\mathbf{F}^{(n)}$, $\mathbf{F}_{RF}^{(n)}$, $\mathbf{\Lambda}^{(n-1)}$, update $\mathbf{F}_{BB}^{(n)}$ using (36).
 - 6: $\mathbf{\Lambda}^{(n)} = \mathbf{\Lambda}^{(n-1)} + \alpha (\mathbf{F}^{(n)} - \mathbf{F}_{RF}^{(n)} \mathbf{F}_{BB}^{(n)})$.
 - 7: Update $\alpha^{(n)}$ according to (37).
 - 8: $n = n + 1$
 - 9: **end while**
 - 10: $\mathbf{F}_{RF}^{(opt)} = \mathbf{F}_{RF}^{(N_{max})}$ and $\mathbf{F}_{BB}^{(opt)} = \mathbf{F}_{BB}^{(N_{max})}$
-

the main computational complexity of the MADMM method is caused by solving three subproblems, i.e. Updating \mathbf{F} , \mathbf{F}_{RF} and \mathbf{F}_{BB} . Updating \mathbf{F} needs complexities of $\mathcal{O}(N_s N_{RF} N_t)$. Using the RCG method updates \mathbf{F}_{RF} with the complexities of $\mathcal{O}(I_1 N_s N_{RF} N_t)$, where I_1 are the number of the iterations required in RCG methods. Updating \mathbf{F}_{BB} needs complexities of $\mathcal{O}(N_{RF}^2 N_t + N_s N_{RF} N_t)$. To summarize, the overall complexity of the MADMM method is $\mathcal{O}(I_0 I_1 N_s N_{RF} N_t)$, where I_0 is the number of MADMM iterations.

V. RIEMANNIAN PRODUCT MANIFOLD BASED HYBRID BEAMFORMING FOR THE PARTIALLY-CONNECTED STRUCTURE

In contract to the fully-connected structure, the partially-connected structure adopts less phase shifters and has lower power and hardware cost in mmWave systems. However, due to the fact that the analog beamformer matrix is a block diagonal structure with the unit modulus, the corresponding optimization problem is hard to tackle. Therefore, in this section, we propose the Riemannian product manifold trust region (RPM-TR) algorithm to design the hybrid beamforming with low-complexity.

A. Problem Reformulation

Due to the special structure of the \mathbf{F}_{RF} , we have the following equality:

$$\|\mathbf{F}_{RF} \mathbf{F}_{BB}\|_F^2 = \frac{N_t}{N_{RF}} \|\mathbf{F}_{BB}\|_F^2 = N_s \quad (38)$$

We note that the relationship between the partially-connected structure and fully-connected can be established as follows,

$$\mathbf{F}_{RF} = \mathbf{F}_{PS} \circ \mathbf{F}_D \quad (39)$$

where $\mathbf{F}_{PS} \in \mathbb{C}^{N_t \times N_{RF}}$ stands for the fully-connected phase shifter matrix, i.e. $|\mathbf{F}_{PS}(i, j)| = 1, \forall i, j$, and $\mathbf{F}_D \in \mathbb{C}^{N_t \times N_{RF}}$ denotes 0-1 connection-state matrix. For the

partially-connected structure, the connection-state matrix is $\mathbf{F}_D = \text{diag}(\mathbf{1}_z, \mathbf{1}_z, \dots, \mathbf{1}_z) \in \mathbb{C}^{N_t \times N_{RF}}$, where $z = \frac{N_t}{N_{RF}}$. Based on the above analysis, the problem (17) can be rewritten as

$$\begin{aligned} \min_{\mathbf{F}_{PS}, \mathbf{F}_{BB}} \quad & \varphi \|(\mathbf{F}_{PS} \circ \mathbf{F}_D) \mathbf{F}_{BB} - \mathbf{F}_{Com}\|_F^2 \\ & + (1 - \varphi) \|(\mathbf{F}_{PS} \circ \mathbf{F}_D) \mathbf{F}_{BB} - \mathbf{F}_{Rad}\|_F^2 \\ \text{s.t.} \quad & \|\mathbf{F}_{BB}\|_F^2 = \frac{N_S N_{RF}}{N_t}, \\ & |\mathbf{F}_{PS}(i, j)| = 1, \forall i, j \end{aligned} \quad (40)$$

For the convenience of deriving the problem, we use the $J(\mathbf{F}_{PS}, \mathbf{F}_{BB})$ denoting the objective function in (40).

B. Geometric Structure of the Riemannian Product Manifold

In order to solve this problem effectively, we recast the constrained optimization problem (40) as an standard optimization form over a product manifold \mathcal{M} , as

$$\min_{(\mathbf{F}_{PS}, \mathbf{F}_{BB}) \in \mathcal{M}} J(\mathbf{F}_{PS}, \mathbf{F}_{BB}) \quad (41)$$

where $\mathcal{M} = \mathcal{M}_{\mathbf{F}_{PS}} \times \mathcal{M}_{\mathbf{F}_{BB}}$ denotes the product manifold of $\mathcal{M}_{\mathbf{F}_{PS}} = \{\mathbf{F}_{PS} \in \mathbb{C}^{N_t \times N_{RF}} : |\mathbf{F}_{PS}(i, j)| = 1, \forall i, j\}$ and $\mathcal{M}_{\mathbf{F}_{BB}} = \{\mathbf{F}_{BB} \in \mathbb{C}^{N_{RF} \times N_S} : \|\mathbf{F}_{BB}\|_F = \sqrt{\frac{N_S N_{RF}}{N_t}}\}$. For the RPM, the tangent space $T_{(\mathbf{F}_{PS}, \mathbf{F}_{BB})} \mathcal{M}$ can be decomposed as a product of two tangent spaces

$$\begin{aligned} T_{(\mathbf{F}_{PS}, \mathbf{F}_{BB})} \mathcal{M} &= T_{\mathbf{F}_{PS}} \mathcal{M}_{\mathbf{F}_{PS}} \times T_{\mathbf{F}_{BB}} \mathcal{M}_{\mathbf{F}_{BB}} \\ &= \{(\zeta_{\mathbf{F}_{PS}}, \zeta_{\mathbf{F}_{BB}}) : \zeta_{\mathbf{F}_{PS}} \in \mathbb{C}^{N_t \times N_{RF}}, \zeta_{\mathbf{F}_{BB}} \in \mathbb{C}^{N_{RF} \times N_S}, \\ & \quad \Re(\zeta_{\mathbf{F}_{PS}} \circ \mathbf{F}_{PS}^*) = \mathbf{0}, \Re(\text{tr}(\mathbf{F}_{BB}^H \zeta_{\mathbf{F}_{BB}})) = 0\} \end{aligned} \quad (42)$$

To facilitate the algorithm development, we need to define the Riemannian gradient over the product manifold, which is calculated as [35]–[37]

$$\begin{aligned} \text{grad} J(\mathbf{F}_{PS}, \mathbf{F}_{BB}) \\ = (\text{grad}_{\mathbf{F}_{PS}} J(\mathbf{F}_{PS}, \mathbf{F}_{BB}), \text{grad}_{\mathbf{F}_{BB}} J(\mathbf{F}_{PS}, \mathbf{F}_{BB})) \end{aligned} \quad (43)$$

where the definition of $\text{grad}_{\mathbf{F}_{PS}} J(\mathbf{F}_{PS}, \mathbf{F}_{BB})$ and $\text{grad}_{\mathbf{F}_{BB}} J(\mathbf{F}_{PS}, \mathbf{F}_{BB})$ and detailed derivations are provided in Appendix A.

Unlike the Riemannian manifold first-order optimization algorithm, for instance, RCG method in section IV, the second-order method adopts the Riemannian Hessian for quadratic information about the objective function, which enjoys more rapid convergence. Thus, to utilize second-order algorithm solving (40), we need derive the explicit expression of the Riemannian Hessian in RPM. The Riemannian Hessian of $J(\mathbf{F}_{PS}, \mathbf{F}_{PS})$ at $(\mathbf{F}_{PS}, \mathbf{F}_{PS}) \in \mathcal{M}$ is a linear operator $\text{Hess}_{(\mathbf{F}_{PS}, \mathbf{F}_{PS})} J : T_{(\mathbf{F}_{PS}, \mathbf{F}_{PS})} \mathcal{M} \mapsto T_{(\mathbf{F}_{PS}, \mathbf{F}_{PS})} \mathcal{M}$ [35]–[37], which are derived in Appendix B.

C. Riemannian Product Manifold Trust Region Algorithm

Based on the above concepts, below we develop the RPM-TR algorithm [35], [36], [38], [44] to solve the problem. Trust region methods [44] can be understood as an enhancement of

Newton's method. Based on [35], [36], the main idea of RPM-TR can be summarized in three steps: 1) Generate a model that is a good approximation of the objective function in a specific region, 2) find the step that minimizes the model function in that specific region, determined by the trust region size, and 3) compute a new iterate based on a retracting mapping.

Firstly, we use a quadratic function to approximate the objective function (40) at the k th iteration with the following form:

$$\begin{aligned} w_k \left(\zeta_{(\mathbf{F}_{PS}, \mathbf{F}_{BB})}^{(k)} \right) \\ = J(\mathbf{F}_{PS}^{(k)}, \mathbf{F}_{BB}^{(k)}) + \left\langle \text{grad} J(\mathbf{F}_{PS}^{(k)}, \mathbf{F}_{BB}^{(k)}), \zeta_{(\mathbf{F}_{PS}, \mathbf{F}_{BB})}^{(k)} \right\rangle \\ + \frac{1}{2} \left\langle \text{Hess} J(\mathbf{F}_{PS}^{(k)}, \mathbf{F}_{BB}^{(k)}) [\zeta_{(\mathbf{F}_{PS}, \mathbf{F}_{BB})}^{(k)}], \zeta_{(\mathbf{F}_{PS}, \mathbf{F}_{BB})}^{(k)} \right\rangle \end{aligned} \quad (44)$$

Furthermore, since the model is only a local approximation of the pullback, we only trust it in a ball around the origin in the tangent space. Thus, in the RPM-TR framework, the update of $(\mathbf{F}_{RF}, \mathbf{F}_{BB})$ within the trust region radius Δ_k is attained by solving

$$\begin{aligned} \min_{(\mathbf{F}_{RF}, \mathbf{F}_{BB})} w_k(\zeta_{(\mathbf{F}_{RF}, \mathbf{F}_{BB})}) \\ \text{s.t.} \quad \langle \zeta_{(\mathbf{F}_{RF}, \mathbf{F}_{BB})}, \zeta_{(\mathbf{F}_{RF}, \mathbf{F}_{BB})} \rangle \leq \Delta_k^2 \end{aligned} \quad (45)$$

Next, an approximate solution $\zeta_{(\mathbf{F}_{PS}, \mathbf{F}_{BB})}^{(k)}$ of the trust region subproblem (45) is computed, for example using a interior point method. Notice that the approximate solution is a local minimum point in tangent space, i.e. $\zeta_{(\mathbf{F}_{PS}, \mathbf{F}_{BB})}^{(k)} \in T_{(\mathbf{F}_{PS}, \mathbf{F}_{BB})} \mathcal{M}$.

Therefore, in the last step, the candidate for the new iterate is obtained by retraction mapping the approximate solution to the product manifold \mathcal{M} , which is

$$(\mathbf{F}_{PS}^{(k)\diamond}, \mathbf{F}_{BB}^{(k)\diamond}) = \mathcal{R}_{(\mathbf{F}_{PS}, \mathbf{F}_{BB})}^{(k)} \left(\zeta_{(\mathbf{F}_{PS}, \mathbf{F}_{BB})}^{(k)} \right) \quad (46)$$

where

$$\mathcal{R}_{(\mathbf{F}_{PS}, \mathbf{F}_{BB})}(\zeta_{(\mathbf{F}_{PS}, \mathbf{F}_{BB})}) = (\mathcal{R}_{\mathbf{F}_{PS}}(\zeta_{\mathbf{F}_{PS}}), \mathcal{R}_{\mathbf{F}_{BB}}(\zeta_{\mathbf{F}_{BB}})) \quad (47)$$

with $\mathcal{R}_{\mathbf{F}_{PS}}(\zeta_{\mathbf{F}_{PS}})$ and $\mathcal{R}_{\mathbf{F}_{BB}}(\zeta_{\mathbf{F}_{BB}})$ being retraction operators on manifold $\mathcal{M}_{\mathbf{F}_{PS}}$ and $\mathcal{M}_{\mathbf{F}_{BB}}$, respectively, and being defined as

$$\mathcal{R}_{\mathbf{F}_{PS}}(\zeta_{\mathbf{F}_{PS}}) = (\mathbf{F}_{PS} + \zeta_{\mathbf{F}_{PS}}) \circ \frac{1}{\|(\mathbf{F}_{PS} + \zeta_{\mathbf{F}_{PS}})\|} \quad (48a)$$

$$\mathcal{R}_{\mathbf{F}_{BB}}(\zeta_{\mathbf{F}_{BB}}) = \sqrt{\frac{N_S N_{RF}}{N_t}} \frac{(\mathbf{F}_{BB} + \zeta_{\mathbf{F}_{BB}})}{\|\mathbf{F}_{BB} + \zeta_{\mathbf{F}_{BB}}\|_F} \quad (48b)$$

Once obtaining the candidate form (46), the quality of the model (44) is assessed by forming the quotient

$$\rho_k = \frac{J(\mathbf{F}_{PS}^{(k)}, \mathbf{F}_{BB}^{(k)}) - J(\mathbf{F}_{PS}^{(k)\diamond}, \mathbf{F}_{BB}^{(k)\diamond})}{w_k(\mathbf{0}_{(\mathbf{F}_{PS}, \mathbf{F}_{BB})}^{(k)}) - w_k(\zeta_{(\mathbf{F}_{PS}, \mathbf{F}_{BB})}^{(k)})} \quad (49)$$

Depending on the value of ρ_k , the candidate $(\mathbf{F}_{PS}^{(k)\diamond}, \mathbf{F}_{BB}^{(k)\diamond})$

will be accepted or discarded and the trust-region radius Δ_{k+1} will be updated [35], [36]. Specifically, a specific procedure is accepted or rejected the $(\mathbf{F}_{PS}^{(k)\diamond}, \mathbf{F}_{BB}^{(k)\diamond})$ based on the rule [35], [36]:

$$(\mathbf{F}_{PS}^{(k+1)}, \mathbf{F}_{BB}^{(k+1)}) = \begin{cases} (\mathbf{F}_{PS}^{(k)\diamond}, \mathbf{F}_{BB}^{(k)\diamond}) & \text{if } \rho_k > \rho' (\text{accept}), \\ (\mathbf{F}_{PS}^{(k)}, \mathbf{F}_{BB}^{(k)}) & \text{otherwise (reject)}. \end{cases} \quad (50)$$

Finally, the trust region radius Δ_{k+1} needs to be updated in each iteration. More concretely, the following update of Δ_{k+1} is used [35], [36], [38]:

$$\Delta_{k+1} = \begin{cases} \frac{1}{4}\Delta_k & \text{if } \rho_k < \frac{1}{4} \\ \min(2\Delta_k, \Delta') & \text{if } \rho_k > \frac{3}{4} \text{ and } \left\| \zeta(\mathbf{F}_{PS}^{(k)}, \mathbf{F}_{BB}^{(k)}) \right\| = \Delta_k \\ \Delta_k & \text{otherwise} \end{cases} \quad (51)$$

According to the above analysis, the proposed RPM-TR algorithm for solving problem (40) is summarized in Algorithm 3.

Algorithm 3 RPM-TR algorithm for partially-connected structure hybrid beamforming design

Require: Initial iteration $(\mathbf{F}_{PS}^{(0)}, \mathbf{F}_{BB}^{(0)}) \in \mathcal{M}$, maximum radius $\Delta' > 0$, reference beamforming matrix \mathbf{F}_{Rad} , \mathbf{F}_{Com} , maximum iterations K_{max} , gradient threshold δ .

Ensure: $\mathbf{F}_{PS}^{(opt)}, \mathbf{F}_{BB}^{(opt)}$.

- 1: **Initialization:** Set $k = 1$, $\Delta_0 \in (0, \Delta')$ and $\rho' \in [0, \frac{1}{4}]$.
 - 2: **for** $k \leq K_{max}$ and $\|\text{grad}J(\mathbf{F}_{PS}, \mathbf{F}_{BB})\|_F > \delta$ **do**
 - 3: Approximately solve the subproblem (45), obtaining $\zeta(\mathbf{F}_{PS}^{(k)}, \mathbf{F}_{BB}^{(k)}) \in T(\mathbf{F}_{PS}^{(k)}, \mathbf{F}_{BB}^{(k)})\mathcal{M}$;
 - 4: Calculate the candidate for next iterate according to (46);
 - 5: Compute the ratio of actual to model improvement using (49);
 - 6: Accept or reject the tentative next iterate depending on the rule (50);
 - 7: Update the trust region radius according to (51);
 - 8: $k = k + 1$;
 - 9: **end for**
 - 10: $\mathbf{F}_{PS}^{(opt)} = \mathbf{F}_{PS}^{(k)}$ and $\mathbf{F}_{BB}^{(opt)} = \mathbf{F}_{BB}^{(k)}$
-

We end this section by analyzing the complexity of the proposed RPM-TR algorithm. For the RPM-TR algorithm, the computational complexity mainly consists of computations of Riemannian gradient and Riemannian Hessian with complexities of $\mathcal{O}(N_t N_{RF} N_s)$ and $\mathcal{O}(N_t N_{RF}^2 + N_t N_{RF} N_s)$, respectively. Hence, the complexity of the algorithm 3 is $\mathcal{O}(I_3(N_t^2 N_{RF} + N_t^2 N_{RF} N_s))$, where I_3 stands for the total iteration numbers of the algorithm.

VI. SIMULATION RESULTS AND DISCUSSION

In this section, several sets of numerical simulations are presented to evaluate the performance of our proposed algorithms. Unless otherwise specified, in all simulations, we

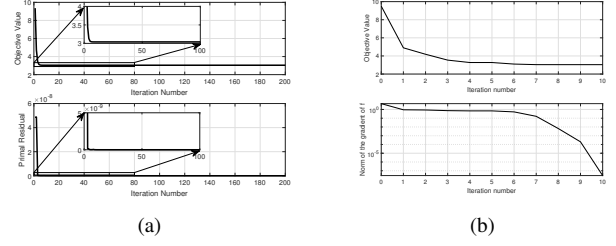


Fig. 3. The convergence performance of the RPM-TR algorithm and MADMM algorithm. (a) The convergence performance of the MADMM algorithm; (b) The convergence performance of the RPM-TR algorithm.

adopt the parameters summarized in Table I. For mmWave channel, the AoAs/DoAs of the all clusters ϕ_{il}^t, ϕ_{il}^r are assumed to be uniformly distributed in $[0, 2\pi)$. As for the MADMM algorithm, we assume the maximum number of iterations is $N_{max} = 200$. The termination criterion of RPM-TR algorithm is the line-search returns a displacement vector smaller than 10^{-6} .

For simplifying notation, we denote the beamformers \mathbf{F}_{Com} and \mathbf{F}_{Rad} as ‘ZF precoder’ and ‘Ref. beampattern’, respectively. For the fully-connected structure, the BCD-based method proposed in [45], [46] is selected as the benchmark for comparison. The alternating minimization (AltMin) algorithm [29] is also included to demonstrate the superiority of the proposed RPM-TR algorithm for the partial-connected structure. We randomly set the same initial point for all methods to provide a fair comparison among different algorithms and structures.

A. Convergence Performance

We first show the resultant convergence performance of the proposed MADMM and RPM-TR in Fig.3. The trade-off parameter for the considered case is set as $\varphi = 0.5$. Fig.3(a) presents the convergence behavior of the MADMM algorithm, which shows that the objective value in (19) increases and converges at a stationary point very fast. Furthermore, the primal residual tend to zero as the iterative process goes on, which verifies the effectiveness of the proposed MADMM algorithm. For the RPM-TR method, in Fig.3(b), the top plot shows the objective function in (40) versus the number of iterations, which illustrates that the objective value decreases with the iteration number. In addition, the norm of the Riemannian gradient displayed in Fig.3(b) bottom tends to 10^{-6} within 10 iterations, which indicates the excellent convergence performance of the RPM-TR algorithm.

B. Spectral Efficiency Performance

In this subsection, we evaluate the downlink communication performance obtained by different algorithms. Fig.4(a) shows the achievable rate as a function of the SNR value and trade-off parameter φ for the fully-connected structure. As expected, the optimal digital precoder can attain the best achievable rate. In addition, the MADMM and BCD achievable rates increase with the SNR value and trade-off parameter. We also find

TABLE I
SIMULATION PARAMETERS

Parameter	Value	Parameter	Value
No. of transmit antennas	$N_t = 32$	No. of RF chains	$N_{RF} = 16$
No. of receive antennas	$N_r = 6$	No. of data streams	$N_s = 6$
No. of rays	$N_{ray} = 5$	No. of clusters	$N_{ray} = 10$

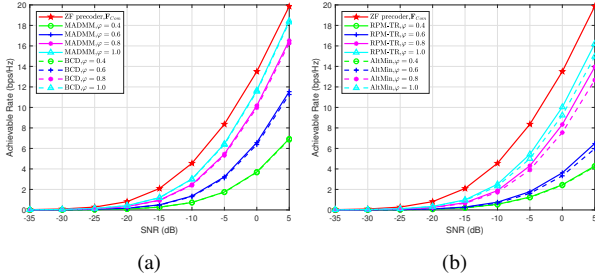


Fig. 4. The achievable rate values versus noise power for different trade-off parameter φ . (a) The achievable rate of the fully-connected structure obtained by MADMM; (b) The achievable rate of the partially-connected structure obtained by RPM-TR

that the MADMM algorithm performs slightly better than the BCD-based method.

Fig.4(b) compares the achievable rate obtained by the RPM-TR method to that by the exiting AltMin algorithm for the partially-connected structure. The result in this figure shows a similar phenomenon to that in Fig.4(a). Moreover, it can be observed that the proposed RPM-TR algorithm outperforms over the AltMin algorithm in terms of the achievable rate.

Furthermore, the comparison between two hybrid beamforming structures show that the partially-structure results in a non-negligible performance loss when comparing with the fully-connected structure.

C. Beampattern Performance

In this subsection, we compare the performance of the achieved beampattern for different algorithms and structures. We assume the targets locate at angle $\{-30^\circ, 30^\circ\}$. Fig.5 reveals that the smaller the trade-off parameter φ is, i.e., the more critical weighting on the radar, the better the sidelobe level of the designed beampattern. On the contrary, the achievable rates of downlink communication get the worse. As a result, a trade-off parameter should be delicately selected to achieve a good balance between communication and radar.

Fig. 6 shows the ISMR performance comparisons of the proposed algorithms with different analog structures. It is seen from the figure that as φ increases, the ISMR properties obtained by all algorithms become worse and worse. Moreover, it is interesting to observe that for $\varphi \leq 0.7$, the algorithms of the partially-connected structure have ISMR behaviors than those of the fully-connected structure, while vice versa for $\varphi \geq 0.8$.

D. Performance With Different RF Chain numbers

In this subsection, we will compare the performance of the two hybrid beamforming structures for different numbers of

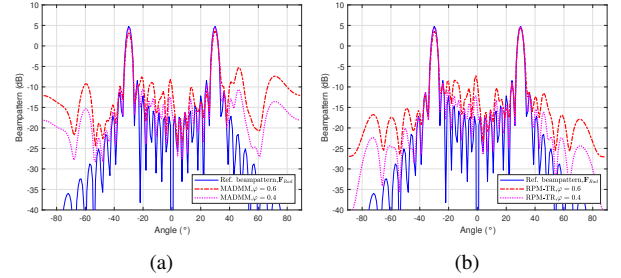


Fig. 5. Radar beampatterns obtained by RPM-TR and MADMM algorithm. (a) Radar beampatterns obtained by MADMM algorithm for fully-connected structure; (b) Radar beampatterns obtained by RPM-TR algorithm for partially-connected structure

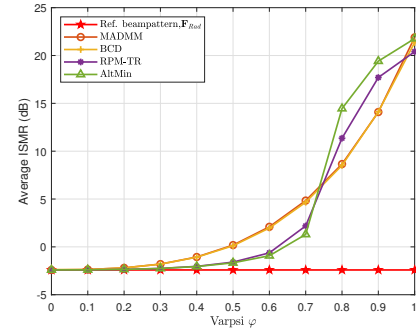


Fig. 6. The ISMR of RPM-TR, AltMin, MADMM and BCD algorithms versus trade-off parameter

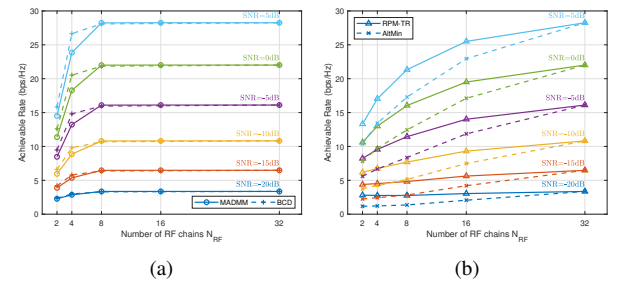


Fig. 7. The spectral efficiency values versus RF chains for different SNR with trade-off parameter $\varphi = 0.4$. (a) Fully-connected structure, (b) Partially-connected structure.

RF chains N_{RF} . We assume the downlink user is equipped with $N_r = 4$ antennas, which is equal to the number of data streams, i.e., $N_s = N_r = 4$.

Fig.7(a) shows the spectral efficiency achieved by the MADMM method as a function of the number of the SNR and N_{RF} for the fully-connected structure. From the figure,

TABLE II
COMPARISONS BETWEEN DIFFERENT HYBRID BEAMFORMERS AND METHODS

Structure	Design approach	No. of PS	Computational complexity	Performance
Fully-connected	MADMM	$N_T N_{RF}$	$\mathcal{O}(I_0 I_1 N_s N_{RF} N_t)$	✓✓✓✓
	BCD	$N_T N_{RF}$	$\mathcal{O}(I_4 (N_s N_{RF}^3 N_t + N_s N_{RF}^2 N_t^2))$	✓✓✓✓
Partially-connected	RPM-TR	N_T	$\mathcal{O}(I_3 (N_t^2 N_{RF} + N_t^2 N_{RF} N_s))$	✓✓✓
	AltMin	N_T	$\mathcal{O}(I_5 (N_t^2 N_s + N_t^2 N_{RF}))$	✓✓

we can see that although the proposed MADMM algorithm is worse than the BCD method when $N_{RF} < 8$, the two methods provide nearly the same results when $N_{RF} \geq 8$. Moreover, we also find that the achievable rates increase with the number of RF chains when $N_{RF} \leq 8$, while the achievable rates are the same and equal to an upper bound when $N_{RF} > 8$. This indicates that it is possible to reduce the number of RF chains in the DFRC system to reduce the hardware cost.

Fig.7(b) displays the achievable spectral efficiency of the proposed hybrid beamforming method for partially-connected structure with different SNR. As expected, for the same SNR, the achievable spectral efficiency increase along with the N_{RF} . Besides, the proposed RPM-TR algorithm consistently outperforms the AltMin method, and the gap becomes smaller with the increasing N_{RF} .

Combing the results in Fig.7(a) and Fig.7(b), we note that the partially-connected structure is more sensitive to the number of N_{RF} compared with a fully-connected one. Thus, choosing an appropriate number of RF chains in practice is essential to balance the performance and the cost.

Finally, the comparisons between different hybrid beamformers and methods are listed in Table II. The results show that although the proposed MADMM is able to achieve nearly identical performance to the BCD approach for the fully-connected structure, it is more computationally efficient. For the partial-connected structure, the proposed RPM-TR outperforms the typical AltMin method in terms of spectral efficiency, and they have similar complexity. For different structures, the fully-connected structure is benefit to improving the DFRC system performance while suffering from a higher hardware complexity.

VII. CONCLUSION

This paper addresses the problems of the hybrid beamforming designs for mmWave DFRC systems with two hybrid beamforming architectures, i.e., the partially-connected and fully-connected structures. The corresponding problems are formulated by the trade-off optimization criterion. To deal with the non-convex formulated problems, we have proposed two low-complexity algorithms, concretely, the MADMM for fully-connected and the RPM-TR for the partially-connected structure, respectively.

The simulation results reveal that the proposed methods can achieve satisfactory radar and communication performance for the DFRC with both fully-connected and partially-connected structures. Besides, the proposed beamforming design provides a flexible trade-off between the radar and communication performance by adjusting a trade-off parameter.

Nevertheless, this initial work only investigates the DFRC system design with manifold optimization, and the particle implementation of these algorithms is still an open problem. Moreover, based on this initial work, there are many issues worth being studied for future research, e.g., the scenarios for radar sensing in the presence of signal-dependent clutters, beam squint aware wideband system, as well as extending the proposed manifold based framework in different scenarios, e.g., reconfigurable intelligent surface aid DFRC.

APPENDIX A

DERIVATION OF RIEMANNIAN GRADIENT

Recalling the Riemannian gradient is calculated as

$$\begin{aligned} \text{grad}J(\mathbf{F}_{PS}, \mathbf{F}_{BB}) \\ = (\text{grad}_{\mathbf{F}_{PS}} J(\mathbf{F}_{PS}, \mathbf{F}_{BB}), \text{grad}_{\mathbf{F}_{BB}} J(\mathbf{F}_{PS}, \mathbf{F}_{BB})) \end{aligned} \quad (52)$$

where the Riemannian gradients $\text{grad}_{\mathbf{F}_{PS}} J(\mathbf{F}_{PS}, \mathbf{F}_{BB})$ and $\text{grad}_{\mathbf{F}_{BB}} J(\mathbf{F}_{PS}, \mathbf{F}_{BB})$ are computed by orthogonal projection from Euclidean space to the tangent space [36] as

$$\begin{aligned} \text{grad}_{\mathbf{F}_{PS}} J(\mathbf{F}_{PS}, \mathbf{F}_{BB}) \\ = \text{Proj}_{\mathbf{F}_{PS}} (\text{Grad}_{\mathbf{F}_{PS}} J(\mathbf{F}_{PS}, \mathbf{F}_{BB})) \\ = \text{Grad}_{\mathbf{F}_{PS}} J(\mathbf{F}_{PS}, \mathbf{F}_{BB}) \\ - \Re\{\text{Grad}_{\mathbf{F}_{PS}} J(\mathbf{F}_{PS}, \mathbf{F}_{BB}) \circ \mathbf{F}_{PS}^* \} \circ \mathbf{F}_{PS} \quad (53a) \\ \text{grad}_{\mathbf{F}_{BB}} J(\mathbf{F}_{PS}, \mathbf{F}_{BB}) \\ = \text{Proj}_{\mathbf{F}_{BB}} (\text{Grad}_{\mathbf{F}_{BB}} J(\mathbf{F}_{PS}, \mathbf{F}_{BB})) \\ = \text{Grad}_{\mathbf{F}_{BB}} J(\mathbf{F}_{PS}, \mathbf{F}_{BB}) \\ - \Re\{\text{tr}(\mathbf{F}_{BB}^H \text{Grad}_{\mathbf{F}_{BB}} J(\mathbf{F}_{PS}, \mathbf{F}_{BB}))\} \mathbf{F}_{BB} \quad (53b) \end{aligned}$$

where $\text{Grad}_{\mathbf{F}_{PS}} J(\mathbf{F}_{PS}, \mathbf{F}_{BB})$ and $\text{Grad}_{\mathbf{F}_{BB}} J(\mathbf{F}_{PS}, \mathbf{F}_{BB})$ denote, respectively, the Euclidean gradients with respect to \mathbf{F}_{PS} and \mathbf{F}_{BB} , and they are calculated as

$$\begin{aligned} \text{Grad}_{\mathbf{F}_{PS}} J(\mathbf{F}_{PS}, \mathbf{F}_{BB}) \\ = 2\varphi \{((\mathbf{F}_D \circ \mathbf{F}_{PS}) \mathbf{F}_{BB} - \mathbf{F}_{Com}) \mathbf{F}_{BB}^H\} \circ \mathbf{F}_D \\ + 2(1 - \varphi) \{((\mathbf{F}_D \circ \mathbf{F}_{PS}) \mathbf{F}_{BB} - \mathbf{F}_{Rad}) \mathbf{F}_{BB}^H\} \circ \mathbf{F}_D \quad (54a) \end{aligned}$$

$$\begin{aligned} \text{Grad}_{\mathbf{F}_{BB}} J(\mathbf{F}_{PS}, \mathbf{F}_{BB}) \\ = 2\varphi(\mathbf{F}_D \circ \mathbf{F}_{PS})^H \{(\mathbf{F}_D \circ \mathbf{F}_{PS}) \mathbf{F}_{BB} - \mathbf{F}_{Com}\} \\ + 2(1 - \varphi)(\mathbf{F}_D \circ \mathbf{F}_{PS})^H \{(\mathbf{F}_D \circ \mathbf{F}_{PS}) \mathbf{F}_{BB} - \mathbf{F}_{Rad}\} \quad (54b) \end{aligned}$$

APPENDIX B

DERIVATION OF RIEMANNIAN HESSIAN

The Riemannian Hessian of $J(\mathbf{F}_{PS}, \mathbf{F}_{PS})$ at $(\mathbf{F}_{PS}, \mathbf{F}_{PS}) \in \mathcal{M}$ is a linear operator $\text{Hess}_{(\mathbf{F}_{PS}, \mathbf{F}_{PS})} J :$

$T_{(\mathbf{F}_{PS}, \mathbf{F}_{BB})} \mathcal{M} \mapsto T_{(\mathbf{F}_{PS}, \mathbf{F}_{BB})} \mathcal{M}$ [35]–[37] defined by

$$\begin{aligned} & \text{Hess}_{(\mathbf{F}_{PS}, \mathbf{F}_{BB})} J(\mathbf{F}_{PS}, \mathbf{F}_{PS}) [\zeta_{(\mathbf{F}_{PS}, \mathbf{F}_{BB})}] \\ &= \nabla_{\zeta_{(\mathbf{F}_{PS}, \mathbf{F}_{BB})}} \text{grad} J(\mathbf{F}_{PS}, \mathbf{F}_{PS}) \end{aligned} \quad (55)$$

for the point $\zeta_{(\mathbf{F}_{PS}, \mathbf{F}_{BB})} \in T_{(\mathbf{F}_{PS}, \mathbf{F}_{BB})} \mathcal{M}$. ∇ denotes the Levi-Civita connection of \mathcal{M} . Specifically, for the RPM, the Riemannian Hessian of $J(\mathbf{F}_{PS}, \mathbf{F}_{PS})$ holds that [36]

$$\begin{aligned} & \text{Hess}_{(\mathbf{F}_{PS}, \mathbf{F}_{BB})} J(\mathbf{F}_{PS}, \mathbf{F}_{PS}) [\zeta_{(\mathbf{F}_{PS}, \mathbf{F}_{BB})}] \\ &= (\text{Hess}_{\mathbf{F}_{PS}} J(\mathbf{F}_{PS}, \mathbf{F}_{PS}) [\zeta_{(\mathbf{F}_{PS}, \mathbf{F}_{BB})}], \\ & \quad \text{Hess}_{\mathbf{F}_{BB}} J(\mathbf{F}_{PS}, \mathbf{F}_{PS}) [\zeta_{(\mathbf{F}_{PS}, \mathbf{F}_{BB})}]) \end{aligned} \quad (56)$$

where $\zeta_{(\mathbf{F}_{PS}, \mathbf{F}_{BB})}$ is tangent vector on the tangent space, i.e. $\zeta_{(\mathbf{F}_{PS}, \mathbf{F}_{BB})} \in T_{(\mathbf{F}_{PS}, \mathbf{F}_{BB})} \mathcal{M}$, $\text{Hess}_{\mathbf{F}_{PS}} J(\mathbf{F}_{PS}, \mathbf{F}_{PS})$ and $\text{Hess}_{\mathbf{F}_{BB}} J(\mathbf{F}_{PS}, \mathbf{F}_{PS})$ denote, respectively, the Riemannian Hessian of $J(\mathbf{F}_{PS}, \mathbf{F}_{PS})$ with respect to \mathbf{F}_{PS} and \mathbf{F}_{PS} . Based on the classical expression of the Levi-Civita connection on a Riemannian submanifold of a Euclidean space [35]–[37], the Riemannian Hessian can be calculated via direction derivative in the embedding space followed by an orthogonal projection to the tangent space. Thus, the Riemannian Hessian $\text{Hess}_{\mathbf{F}_{PS}} J(\mathbf{F}_{PS}, \mathbf{F}_{PS})$ and $\text{Hess}_{\mathbf{F}_{BB}} J(\mathbf{F}_{PS}, \mathbf{F}_{PS})$ are computed as [38], [40]

$$\begin{aligned} & \text{Hess}_{\mathbf{F}_{PS}} J(\mathbf{F}_{PS}, \mathbf{F}_{PS}) [\zeta_{(\mathbf{F}_{PS}, \mathbf{F}_{BB})}] \\ &= \nabla_{\zeta_{\mathbf{F}_{PS}}} \text{grad} J(\mathbf{F}_{PS}, \mathbf{F}_{PS}) \\ &= \text{Proj}_{\mathbf{F}_{PS}} (\text{Dgrad}_{\mathbf{F}_{PS}} J(\mathbf{F}_{PS}, \mathbf{F}_{PS}) [\zeta_{(\mathbf{F}_{PS}, \mathbf{F}_{BB})}]) \\ &= \text{Proj}_{\mathbf{F}_{PS}} (\text{eHess}_{\mathbf{F}_{PS}} J - \Re \{ \mathbf{F}_{PS} \circ (\text{Grad}_{\mathbf{F}_{PS}} J)^* \} \circ \zeta_{\mathbf{F}_{PS}}) \end{aligned} \quad (57a)$$

$$\begin{aligned} & \text{Hess}_{\mathbf{F}_{BB}} J(\mathbf{F}_{PS}, \mathbf{F}_{PS}) [\zeta_{(\mathbf{F}_{PS}, \mathbf{F}_{BB})}] \\ &= \nabla_{\zeta_{\mathbf{F}_{BB}}} \text{grad} J(\mathbf{F}_{PS}, \mathbf{F}_{PS}) \\ &= \text{Proj}_{\mathbf{F}_{BB}} (\text{Dgrad}_{\mathbf{F}_{BB}} J(\mathbf{F}_{PS}, \mathbf{F}_{PS}) [\zeta_{(\mathbf{F}_{PS}, \mathbf{F}_{BB})}]) \\ &= \text{Proj}_{\mathbf{F}_{BB}} (\text{eHess}_{\mathbf{F}_{BB}} J) + \Re \{ \text{tr} (\mathbf{F}_{BB}^H \text{Grad}_{\mathbf{F}_{BB}} J) \} \zeta_{\mathbf{F}_{BB}} \end{aligned} \quad (57b)$$

where $\text{Dgrad}_{\mathbf{F}_{PS}} J(\mathbf{F}_{PS}, \mathbf{F}_{PS}) [\zeta_{(\mathbf{F}_{PS}, \mathbf{F}_{BB})}]$ and $\text{Dgrad}_{\mathbf{F}_{BB}} J(\mathbf{F}_{PS}, \mathbf{F}_{PS}) [\zeta_{(\mathbf{F}_{PS}, \mathbf{F}_{BB})}]$ are the directional derivative of the Riemannian gradient $\text{grad}_{\mathbf{F}_{PS}} J(\mathbf{F}_{PS}, \mathbf{F}_{PS})$ and $\text{grad}_{\mathbf{F}_{BB}} J(\mathbf{F}_{PS}, \mathbf{F}_{PS})$, the Euclidean Hessian $\text{eHess}_{\mathbf{F}_{PS}} J$ and $\text{eHess}_{\mathbf{F}_{BB}} J$ denote, respectively, the directional derivative of the Euclidean gradient (54a) and (54b), which are computed as

$$\begin{aligned} & \text{eHess}_{\mathbf{F}_{PS}} J \\ &= 2\varphi \{ ((\mathbf{F}_D \circ \mathbf{F}_{PS}) \mathbf{F}_{BB} - \mathbf{F}_{Com}) \zeta_{BB}^H \} \circ \mathbf{F}_D \\ & \quad + 2(1 - \varphi) \{ ((\mathbf{F}_D \circ \mathbf{F}_{PS}) \mathbf{F}_{BB} - \mathbf{F}_{Rad}) \zeta_{BB}^H \} \circ \mathbf{F}_D \\ & \quad + 2 \{ ((\mathbf{F}_D \circ \zeta_{PS}) \mathbf{F}_{BB} + (\mathbf{F}_D \circ \mathbf{F}_{PS}) \zeta_{BB}) \mathbf{F}_{BB}^H \} \circ \mathbf{F}_D \\ & \text{eHess}_{\mathbf{F}_{BB}} J \\ &= 2\varphi (\mathbf{F}_D \circ \zeta_{PS})^H \{ (\mathbf{F}_D \circ \mathbf{F}_{PS}) \mathbf{F}_{BB} - \mathbf{F}_{Com} \} \\ & \quad + 2(1 - \varphi) (\mathbf{F}_D \circ \zeta_{PS})^H \{ (\mathbf{F}_D \circ \mathbf{F}_{PS}) \mathbf{F}_{BB} - \mathbf{F}_{Rad} \} \\ & \quad + 2(\mathbf{F}_D \circ \mathbf{F}_{PS})^H \{ (\mathbf{F}_D \circ \zeta_{PS}) \mathbf{F}_{BB} + (\mathbf{F}_D \circ \mathbf{F}_{PS}) \zeta_{BB} \} \end{aligned}$$

REFERENCES

- [1] R. Saruthirathanaworakun, J. M. Peha, and L. M. Correia, "Opportunistic sharing between rotating radar and cellular," *IEEE Journal on Selected Areas in Communications*, vol. 30, no. 10, pp. 1900–1910, 2012.
- [2] J. A. Mahal, A. Khawar, A. Abdelhadi, and T. C. Clancy, "Spectral coexistence of MIMO radar and MIMO cellular system," *IEEE Transactions on Aerospace and Electronic Systems*, vol. 53, no. 2, pp. 655–668, 2017.
- [3] Z. Cheng, B. Liao, Z. He, Y. Li, and J. Li, "Spectrally compatible waveform design for MIMO radar in the presence of multiple targets," *IEEE Transactions on Signal Processing*, vol. 66, no. 13, pp. 3543–3555, 2018.
- [4] A. Aubry, A. De Maio, M. Piezzo, and A. Farina, "Radar waveform design in a spectrally crowded environment via nonconvex quadratic optimization," *IEEE Transactions on Aerospace and Electronic Systems*, vol. 50, no. 2, pp. 1138–1152, 2014.
- [5] C. Nunn and L. R. Moyer, "Spectrally-compliant waveforms for wide-band radar," *IEEE Aerospace and Electronic Systems Magazine*, vol. 27, no. 8, pp. 11–15, 2012.
- [6] B. Li, A. P. Petropulu, and W. Trappe, "Optimum co-design for spectrum sharing between matrix completion based MIMO radars and a MIMO communication system," *IEEE Transactions on Signal Processing*, vol. 64, no. 17, pp. 4562–4575, 2016.
- [7] B. Li and A. P. Petropulu, "Joint transmit designs for coexistence of MIMO wireless communications and sparse sensing radars in clutter," *IEEE Transactions on Aerospace and Electronic Systems*, vol. 53, no. 6, pp. 2846–2864, 2017.
- [8] F. Liu, C. Masouros, A. Li, H. Sun, and L. Hanzo, "MU-MIMO communications with MIMO radar: From co-existence to joint transmission," *IEEE Transactions on Wireless Communications*, vol. 17, no. 4, pp. 2755–2770, 2018.
- [9] L. Zheng, M. Lops, and X. Wang, "Adaptive interference removal for uncoordinated radar/communication coexistence," *IEEE Journal of Selected Topics in Signal Processing*, vol. 12, no. 1, pp. 45–60, 2018.
- [10] F. Liu, C. Masouros, A. Li, T. Ratnarajah, and J. Zhou, "MIMO radar and cellular coexistence: A power-efficient approach enabled by interference exploitation," *IEEE Transactions on Signal Processing*, vol. 66, no. 14, pp. 3681–3695, 2018.
- [11] N. Nartasilpa, A. Salim, D. Tuninetti, and N. Devroye, "Communications system performance and design in the presence of radar interference," *IEEE Transactions on Communications*, vol. 66, no. 9, pp. 4170–4185, 2018.
- [12] M. Coccia and J. Watts, "A theory of the evolution of technology: Technological parasitism and the implications for innovation management," *Journal of Engineering and Technology Management*, vol. 55, p. 101552, 2020.
- [13] M. Coccia, "An introduction to the methods of inquiry in social sciences," *Journal of Social and Administrative Sciences*, vol. 5, no. 2, pp. 116–126, 2018.
- [14] C. Sturm and W. Wiesbeck, "Waveform design and signal processing aspects for fusion of wireless communications and radar sensing," *Proceedings of the IEEE*, vol. 99, no. 7, pp. 1236–1259, 2011.
- [15] S. D. Blunt, M. R. Cook, and J. Stiles, "Embedding information into radar emissions via waveform implementation," in *2010 International waveform diversity and design conference*. IEEE, 2010, pp. 000 195–000 199.
- [16] K. Wu, J. A. Zhang, X. Huang, and Y. J. Guo, "Frequency-hopping mimo radar-based communications: An overview," *IEEE Aerospace and Electronic Systems Magazine*, 2021.
- [17] F. Liu, L. Zhou, C. Masouros, A. Li, W. Luo, and A. P. Petropulu, "Toward dual-functional radar-communication systems: Optimal waveform design," *IEEE Transactions on Signal Processing*, vol. 66, no. 16, pp. 4264–4279, 2018.
- [18] S. D. Blunt, P. Yatham, and J. Stiles, "Intrapulse radar-embedded communications," *IEEE Transactions on Aerospace and Electronic Systems*, vol. 46, no. 3, pp. 1185–1200, 2010.
- [19] D. Ciuonzo, A. De Maio, G. Foglia, and M. Piezzo, "Intrapulse radar-embedded communications via multiobjective optimization," *IEEE Transactions on Aerospace and Electronic Systems*, vol. 51, no. 4, pp. 2960–2974, 2015.
- [20] T. Wei, L. Wu, K. V. Mishra, and M. B. Shankar, "Multiple irs-assisted wideband dual-function radar-communication," *2022 2nd IEEE International Symposium on Joint Communications & Sensing (JC&S)*, pp. 1–5, 2022.
- [21] T. Tian, G. Li, H. Deng, and J. Lu, "Adaptive bit/power allocation with beamforming for dual-function radar-communication," *IEEE Wireless Communications Letters*, 2022.
- [22] Z. Xiao and Y. Zeng, "Waveform design and performance analysis for full-duplex integrated sensing and communication," *IEEE Journal on Selected Areas in Communications*, vol. 40, no. 6, pp. 1823–1837, 2022.

- [23] Z. Huang, B. Tang, C. Huang, and L. Qin, "Direct transmit waveform design to match a desired beampattern under the constant modulus constraint," *Digital Signal Processing*, vol. 126, p. 103486, 2022.
- [24] X. Gao, L. Dai, and A. M. Sayeed, "Low rf-complexity technologies to enable millimeter-wave mimo with large antenna array for 5g wireless communications," *IEEE Communications Magazine*, vol. 56, no. 4, pp. 211–217, 2018.
- [25] S. Han, I. Chih-Lin, Z. Xu, and C. Rowell, "Large-scale antenna systems with hybrid analog and digital beamforming for millimeter wave 5g," *IEEE Communications Magazine*, vol. 53, no. 1, pp. 186–194, 2015.
- [26] A. F. Molisch, V. V. Ratnam, S. Han, Z. Li, S. L. H. Nguyen, L. Li, and K. Haneda, "Hybrid beamforming for massive mimo: A survey," *IEEE Communications magazine*, vol. 55, no. 9, pp. 134–141, 2017.
- [27] I. Ahmed, H. Khammari, A. Shahid, A. Musa, K. S. Kim, E. De Poorter, and I. Moerman, "A survey on hybrid beamforming techniques in 5g: Architecture and system model perspectives," *IEEE Communications Surveys & Tutorials*, vol. 20, no. 4, pp. 3060–3097, 2018.
- [28] R. W. Heath, N. Gonzalez-Prelcic, S. Rangan, W. Roh, and A. M. Sayeed, "An overview of signal processing techniques for millimeter wave mimo systems," *IEEE journal of selected topics in signal processing*, vol. 10, no. 3, pp. 436–453, 2016.
- [29] X. Yu, J. Shen, J. Zhang, and K. B. Letaief, "Alternating minimization algorithms for hybrid precoding in millimeter wave MIMO systems," *IEEE Journal of Selected Topics in Signal Processing*, vol. 10, no. 3, pp. 485–500, 2016.
- [30] F. Liu and C. Masouros, "Hybrid beamforming with sub-arrayed mimo radar: Enabling joint sensing and communication at mmwave band," in *ICASSP 2019-2019 IEEE International Conference on Acoustics, Speech and Signal Processing (ICASSP)*. IEEE, 2019, pp. 7770–7774.
- [31] Z. Cheng, J. He, S. Shi, Z. He, and B. Liao, "Hybrid beamforming for wideband ofdm dual function radar communications," in *ICASSP 2021-2021 IEEE International Conference on Acoustics, Speech and Signal Processing (ICASSP)*. IEEE, 2021, pp. 8238–8242.
- [32] Z. Cheng, Z. He, and B. Liao, "Hybrid beamforming for multi-carrier dual-function radar-communication system," *IEEE Transactions on Cognitive Communications and Networking*, pp. 1–1, 2021.
- [33] F. Liu, C. Masouros, A. P. Petropulu, H. Griffiths, and L. Hanzo, "Joint radar and communication design: Applications, state-of-the-art, and the road ahead," *IEEE Transactions on Communications*, vol. 68, no. 6, pp. 3834–3862, 2020.
- [34] B. Wang, L. Wu, Z. Cheng, and Z. He, "Exploiting constructive interference in symbol level hybrid beamforming for dual-function radar-communication system," *IEEE Wireless Communications Letters*, pp. 1–1, 2022.
- [35] N. Boumal, "An introduction to optimization on smooth manifolds," *Available online*, May, 2020.
- [36] P.-A. Absil, R. Mahony, and R. Sepulchre, *Optimization algorithms on matrix manifolds*. Princeton University Press, 2009.
- [37] C. Udriste, *Convex functions and optimization methods on Riemannian manifolds*. Springer Science & Business Media, 2013, vol. 297.
- [38] J. Li, G. Liao, Y. Huang, Z. Zhang, and A. Nehorai, "Riemannian geometric optimization methods for joint design of transmit sequence and receive filter on MIMO radar," *IEEE Transactions on Signal Processing*, vol. 68, pp. 5602–5616, 2020.
- [39] J. Nocedal and S. Wright, *Numerical optimization*. Springer Science & Business Media, 2006.
- [40] P.-A. Absil, R. Mahony, and J. Trumpf, "An extrinsic look at the riemannian hessian," in *International conference on geometric science of information*. Springer, 2013, pp. 361–368.
- [41] Z. Cheng, B. Liao, Z. He, J. Li, and J. Xie, "Joint design of the transmit and receive beamforming in MIMO radar systems," *IEEE Transactions on Vehicular Technology*, vol. 68, no. 8, pp. 7919–7930, 2019.
- [42] H. Xu, R. S. Blum, J. Wang, and J. Yuan, "Colocated MIMO radar waveform design for transmit beampattern formation," *IEEE Transactions on Aerospace and Electronic Systems*, vol. 51, no. 2, pp. 1558–1568, 2015.
- [43] S. Boyd, N. Parikh, and E. Chu, *Distributed optimization and statistical learning via the alternating direction method of multipliers*. Now Publishers Inc, 2011.
- [44] A. R. Conn, N. I. Gould, and P. L. Toint, *Trust region methods*. SIAM, 2000.
- [45] P. Richtárik and M. Takáč, "Distributed coordinate descent method for learning with big data," *The Journal of Machine Learning Research*, vol. 17, no. 1, pp. 2657–2681, 2016.
- [46] Z.-Q. Luo and P. Tseng, "On the convergence of the coordinate descent method for convex differentiable minimization," *Journal of Optimization Theory and Applications*, vol. 72, no. 1, pp. 7–35, 1992.